

Deep Dilated Convolutional Nets for the Automatic Segmentation of Retinal Vessels

Ali Hatamizadeh¹, Hamid Hosseini², Zhengyuan Liu¹, Steven D. Schwartz²,
and Demetri Terzopoulos¹

¹ Computer Science Department, Henry Samueli School of Engineering

² Stein Eye Institute, David Geffen School of Medicine
University of California, Los Angeles, CA 90095, USA

Abstract. The reliable segmentation of retinal vasculature can provide the means to diagnose and monitor the progression of a variety of diseases affecting the blood vessel network, including diabetes and hypertension. We leverage the power of convolutional neural networks to devise a reliable and fully automated method that can accurately detect, segment, and analyze retinal vessels. In particular, we propose a novel, fully convolutional deep neural network with an encoder-decoder architecture that employs dilated spatial pyramid pooling with multiple dilation rates to recover the lost content in the encoder and add multiscale contextual information to the decoder. We also propose a simple yet effective way of quantifying and tracking the widths of retinal vessels through direct use of the segmentation predictions. Unlike previous deep-learning-based approaches to retinal vessel segmentation that mainly rely on patch-wise analysis, our proposed method leverages a whole-image approach during training and inference, resulting in more efficient training and faster inference through the access of global content in the image. We have tested our method on three publicly available datasets, and our state-of-the-art results on both the DRIVE and CHASE-DB1 datasets attest to the effectiveness of our approach.

Keywords: Retina Vessel Segmentation · Width Estimation · Dilated Spatial Pyramid Pooling · Convolutional Neural Networks · Deep Learning.

1 Introduction

The retina and its vasculature are directly visible due to the optically clear media of the human eye. As the only part of the central nervous system that can be rapidly and non-invasively imaged with a variety of modalities in the out-patient setting, the retina provides a window into the human body, thus offering the opportunity to assess changes associated with systemic diseases such as hypertension, diabetes, and neurodegenerative disorders. The sequelae of these conditions, specifically stroke, heart disease, and dementia represent major causes of morbidity and mortality in the developed world. To date, all classification schemes for retinal vascular changes in these conditions, particularly in the early stages

of disease, have been based on qualitative changes based on human assessment. We and others hypothesize that biomarkers of seriously adverse health events exist in the quantitative assessment of retinal vasculature changes associated with early, even asymptomatic, diabetes, hypertension, or neurodegenerations. Specifically, high blood pressure, for example, causes structural changes in the macro- and micro-vasculature of vital organs throughout the body, including the brain, heart, and kidney. The retinal vasculature is similarly impacted but has the advantage of accessibility to multimodal imaging, providing the opportunity to quantitatively assess prognosis, risk, and response to treatment. Narrowing of retinal vessels has been described as an early, classic sign of hypertension. However, this early sign is difficult to use in everyday clinical practice, which usually includes only non-quantitative, subjective visual assessment of the retina by examination, photograph, or even angiography. An automated, quantitative, reliable, reproducible tool that measures changes in the retinal vasculature in response to disease and intervention might augment and disrupt current evaluation and treatment paradigms by allowing physicians to detect disease, predict outcomes, and assess interventions much earlier in the course of disease, thereby opening the potential for improved outcomes in major unmet public health needs.

A critical step in tracking important structural changes of the retinal vasculature is segmentation of the retinal vessels, as it enables locating the veins and arteries and extracting relevant information such as a profile of the width changes of the vessels. Since the manual segmentation of vessels by clinicians is a notoriously laborious and error-prone process, it is important to establish fully automated and reliable segmentation methods that can be leveraged for extracting the aforementioned information with minimal supervision.

Since the advent of deep learning, Convolutional Neural Networks (CNNs) have become popular due to their powerful, nonlinear feature extraction capabilities in many computer vision related applications [5, 7, 14, 2]. Several researchers have applied CNNs to the task of retinal vessel segmentation in fundus images. However, most are patch-wise methods that ignore the global context in the image and are usually inefficient during inference. Melinščak et al. [11] employed a simple 10-layer CNN architecture based on a patch-wise technique, but their results suffer from low sensitivity in comparison to other techniques. Fu et al. [4] treated the problem of segmentation as a boundary detection problem and combined a CNN with a conditional random field to address the segmentation of retinal vessels, but their method is slower than whole-image CNNs and is outperformed by a number of other proposed methods in different metrics. Zhuang [16] proposed an architecture based on U-Net [13], which utilizes multiple-path networks that leverages a path-wise formulation in segmenting retinal vessels.

In the present paper, we exploit the power of CNNs to create a reliable, fully automated, method that can accurately detect and segment retinal vessels, and we devise an algorithm for the automatic quantification of widths in retinal vessels directly from the segmentation masks, which can be employed toward the creation the aforementioned biomarkers. In particular, we introduce an encoder-decoder CNN architecture that leverages a new dilated spatial pyra-

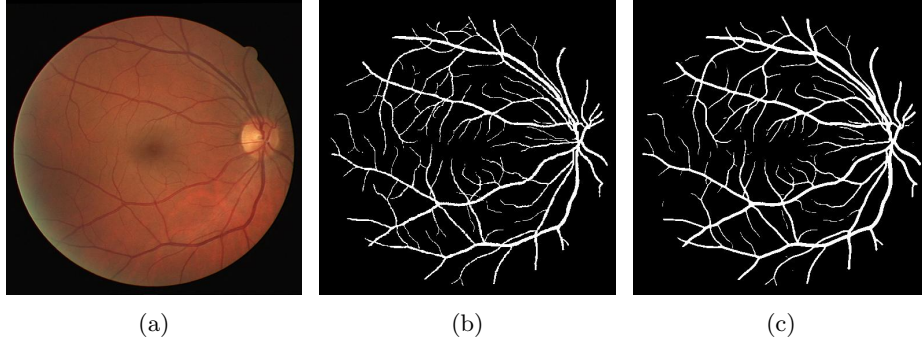


Fig. 1: Segmentation of an image from the DRIVE dataset. (a) Input image. (b) Ground truth. (c) Segmentation prediction output by our network.

mid pooling with multiple dilation rates, which preserves resolution yet adds multiscale information to the decoder. Figure 1 shows an input fundus image with its corresponding ground-truth and the vascular segmentation output by our network.

2 Method

2.1 Vessel Segmentation

We propose a fully convolutional encoder-decoder architecture, as depicted in Figure 2, which leverages dilated residual blocks along with deep supervision at multiple scales for effectively learning the multiresolution details of retinal vessels. Each convolutional layer with kernel W is followed by a rectified linear unit (ReLU) $Re(X) = \max(0, X)$ and a batch normalization $BN_{\gamma, \beta}(X)$ with parameters γ, β that are learned during training. Consequently, every location i in the output of a convolutional layer followed by ReLU and batch normalization can be represented as

$$Y(i) = BN_{\gamma, \beta}(Re(\sum_{j=1} X[i + j \cdot r]W[j])), \quad (1)$$

where r is the dilation rate. We employ both standard and dilated convolutional layers for which the value of r in the former is 1 and in the latter depends on where it is used. In this work, we utilize dilated residual blocks that consist of two consecutive dilated convolutional layers whose outputs are fused with the input.

Our encoder-decoder architecture spans four different resolutions. In the encoder, each path consist of 2 consecutive 3×3 convolutional layers, followed by a dilated residual unit with a dilation rate of 2. Before being fed into the dilated residual unit, the output of these convolutional layers are added with the output

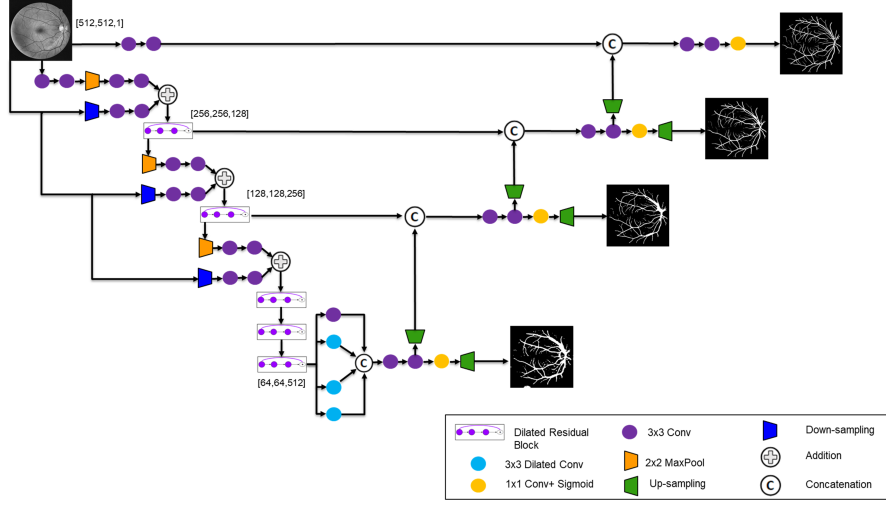


Fig. 2: Our proposed fully convolutional architecture. Dilated spatial pyramid pooling aggregates the outputs of the multiple stages.

feature maps of another 2 consecutive 3×3 convolutional layers that learn additional multiscale information from the re-sized input image in that resolution. At the third stage of our architecture, we utilize a series of 3 consecutive dilated residual blocks with dilation rates of 1, 2, and 4, respectively. Finally, we incorporate a dilated spatial pyramid pooling layer with 4 different dilation rates of 1, 6, 12 and 18 in order to recover the content lost in the learned feature maps during the encoding process.

Subsequently, the decoder in our architecture receives the learned multiscale contextual information of the dilated spatial pyramid pooling layer and is connected to the dilated residual units at each resolution via skip connections. In each path of the decoder, the image is up-sampled and 2 consecutive 3×3 convolutional layers are used before proceeding to the next resolution. Moreover, each scale branches to an additional convolutional layer whose output is resized to the original input image size and is followed by another convolutional layer with sigmoid activation function.

These multiscale prediction maps contribute to the final loss layer. We utilize a soft Srensen-Dice loss function as our basis and aggregate throughout each of the four resolutions:

$$Loss = \sum_{m=1}^4 \left(1 - \sum_{n=1}^N \frac{2G_n P_{n,m}}{G_n + P_{n,m} + \epsilon} \right) + \lambda \|w\|_2^2, \quad (2)$$

where N , $P_{n,m}$, and G_n denote the total number of pixels, the label prediction of pixel n in scale m , and the ground truth label of pixel n , respectively, ϵ is a smoothing constant, and λ is the weight decay regularization hyper-parameter.

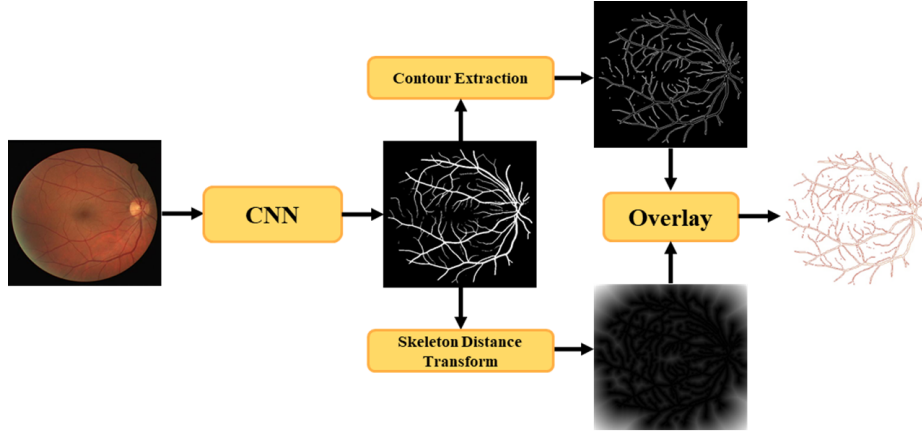


Fig. 3: Estimating the width profile of retinal vessels from segmentation.

2.2 Vessel Width Estimation

We propose a simple, yet effective method for the automatic estimation of vessel width profiles by leveraging the segmentation masks obtained by our CNN. Similar to [15], we first obtain the skeleton of the image by successively identifying the borderline pixels and removing the corresponding pixels that maintain the connectivity of the vessels. This operation approximates the center line of the vessel and represents its topology. We then calculate the distance of each pixel to the derived center-lines by applying an Euclidean distance transform to the generated feature map. Finally, we extract the contour of the original segmentation mask and overlay the generated distance transform onto this map to create the final width map of the retinal vessels. Needless to say, our formulation is only valid in areas where these vessels exist, otherwise the width value is set to zero. Figure 3 illustrates our width estimation algorithm in more detail. Unlike competing methods, our method does not rely on hand-crafted geometric equations nor on user interaction.

3 Experiments

3.1 Implementation Details

We have implemented our CNN in TensorFlow [1]. All the input images are converted to gray-scale, transformed by contrast-limited adaptive histogram equalization, resized to a predefined size of 512×512 , and intensity normalized between 0 and 1. Our model is trained, with a batch size of 2, on an Nvidia Titan XP GPU and an Intel Core i7-7700K CPU @ 4.20GHz. We use the Adam optimization algorithm with an initial learning rate of 0.001 and exponentially decay its rate. The smoothing constant in the loss function and the weight decay hyperparameter are set to 10^{-5} and 0.0008, respectively. Since the number of images

Table 1: Segmentation Evaluations on the DRIVE and CHASE-DB1 datasets.

Method	DRIVE				CHASE-DB1			
	SE	SP	Acc	F1	SE	SP	Acc	F1
Melinščak et al. [11]	0.7276	0.9785	0.9466	-	-	-	-	-
Li et al. [9]	0.7569	0.9816	0.9527	-	0.7507	0.9793	0.9581	-
Liskowski et al. [10]	0.7520	0.9806	0.9515	-	-	-	-	-
Fu et al. [4]	0.7603	-	0.9523	-	0.7130	-	0.9489	-
Oliveira et al. [12]	0.8039	0.9804	0.9576	-	0.7779	0.9864	0.9653	-
M2U-Net [8]	-	-	0.9630	0.8091	-	-	0.9703	0.8006
U-Net [3]	0.7537	0.9820	0.9531	0.8142	0.8288	0.9701	0.9578	0.7783
Recurrent U-Net [3]	0.7751	0.9816	0.9556	0.8155	0.7459	0.9836	0.9622	0.7810
R2U-Net [3]	0.7792	0.9816	0.9556	0.8171	0.7756	0.9820	0.9634	0.7928
LadderNet [16]	0.7856	0.9810	0.9561	0.8202	0.7978	0.9818	0.9656	0.8031
DUNet [6]	0.7894	0.9870	0.9697	0.8203	0.8229	0.9821	0.9724	0.7853
Ours	0.8197	0.9819	0.9686	0.8223	0.8300	0.9848	0.9750	0.8073

is limited, we perform common data augmentation techniques such as rotating, flipping horizontally and vertically, and transposing the image.

3.2 Datasets

We have tested our model on two publicly available retinal vessel segmentation datasets—DRIVE and CHASE-DB1. The DRIVE dataset consists of 40 two-dimensional RGB images with each image having a resolution of 565×584 pixels, divided into a training set and test set, each comprising 20 images. The CHASE-DB1 dataset includes 28 images, collected from both eyes of 14 children. Each image has a resolution of 999×960 pixels. We divided the CHASE-DB1 dataset into a training set of 20 images and a testing set of 8 images.

3.3 Results

We used the following metrics to measure the performance of our model: With TP , TN , FP , FN denoting true positive, true negative, false positive, and false negative, respectively, the sensitivity and specificity are given as

$$SE = \frac{TP}{TP + FN}, \quad SP = \frac{TN}{TN + FP}, \quad (3)$$

the accuracy and precision as

$$Acc = \frac{TP + TN}{TP + TN + FP + FN}, \quad Precision = \frac{TP}{TP + FP}, \quad (4)$$

and the recall as

$$Recall = \frac{TP}{TP + FN}. \quad (5)$$

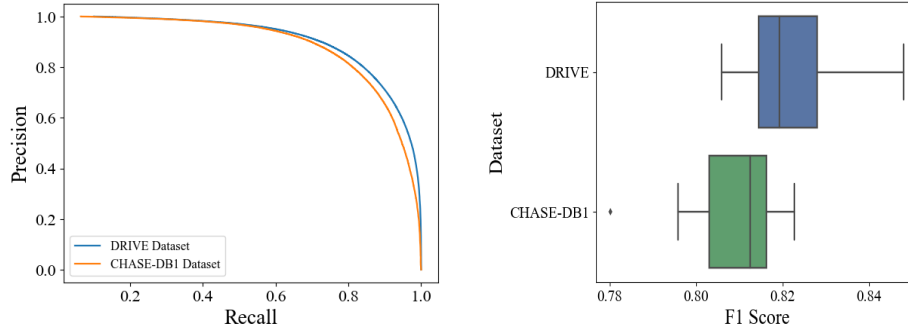


Fig. 4: Evaluation of our model’s performance on the DRIVE and CHASE-DB1 datasets.

The score

$$F1 = 2 \times \frac{Precision \times Recall}{Precision + Recall} \quad (6)$$

is the same as the Dice coefficient.

Table 1 compares to competing methods the performance of our model on the DRIVE and CHASE-DB1 datasets. On the DRIVE dataset, our model exceeds the state-of-the-art performance on the F1 score and sensitivity while being very competitive to [6] in specificity and accuracy. Figure 4 presents the precision-recall curve as well as the box and whisker plot of our model’s performance on the DRIVE dataset. The F1 scores are between 0.80 to 0.84 with no outliers falling outside the interquartile range.

In addition, for the CHASE-DB1 dataset our model exceeds the state-of-the-art performance for all metrics except specificity, for which [12] performs slightly better. The F1 scores are between 0.78 to 0.82. The precision-recall curve in Figure 4 demonstrates a similar performance on both the DRIVE and CHASE-DB1 datasets with a marginal lead for the latter dataset.

For 4 images from the DRIVE dataset and 2 images from the CHASE-DB1 dataset, Figure 5 demonstrates the final segmentation of our model compared to the masks that were manually created by clinicians as well as the generated width profiles. Clearly, our model successfully captures the intricate arteries and veins without the presence of any additional false positives as are present in the outputs of the competing methods.

4 Discussion

Our substantially improved state-of-the-art results on two publicly available datasets, DRIVE and CHASE-DB1, confirm the effectiveness of our model. Unlike the competing patch-wise approaches, our method operates on the entire image. This has proven to be beneficial as our model is significantly faster than

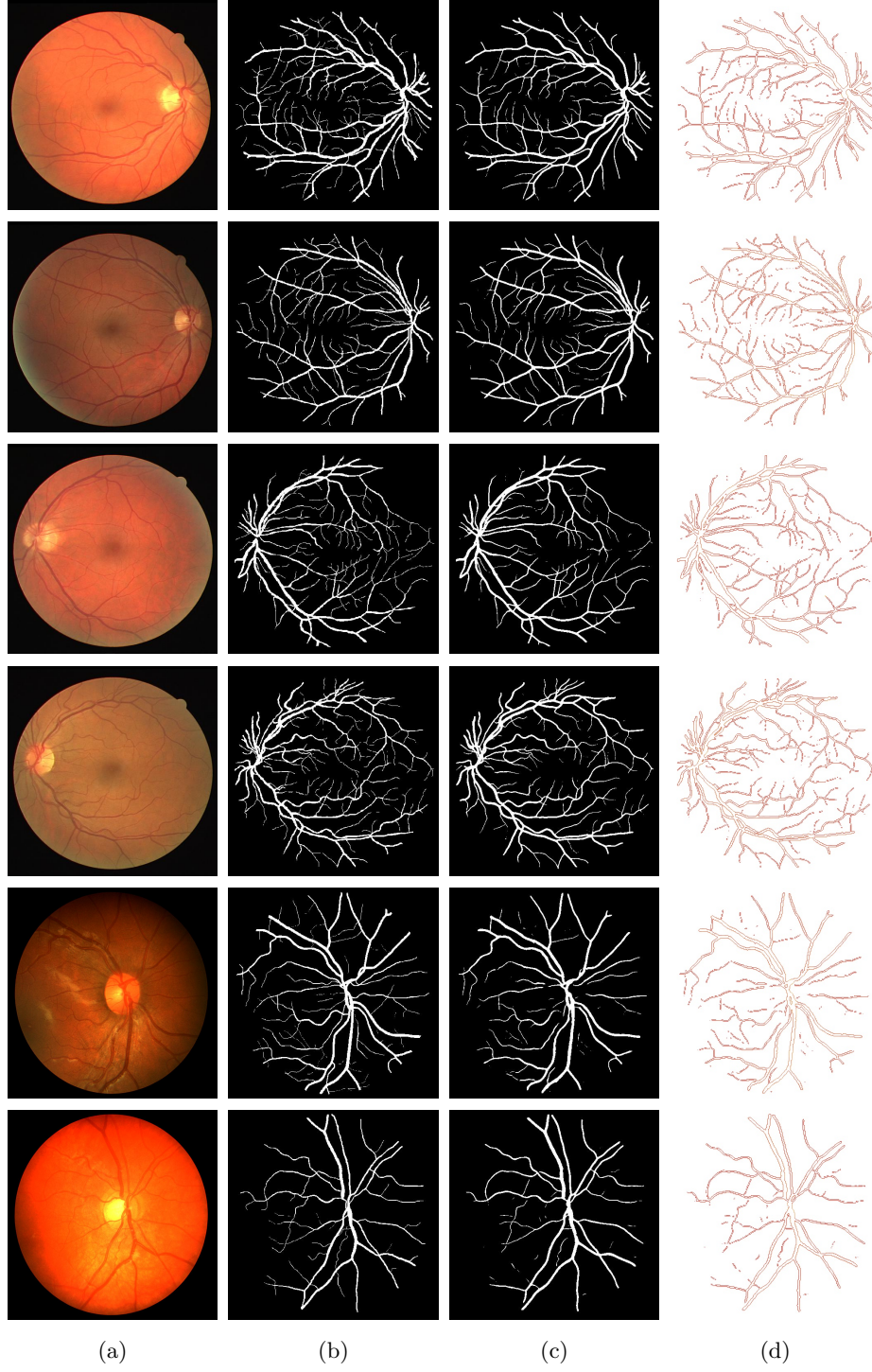


Fig. 5: (a) Input images (rows 1–4 from DRIVE; rows 5–6 from CHASE-DB1), (b) labels, (c) segmentations, (d) width estimation profiles.

the patch-wise approaches that must slide moving windows of multiple sizes over the image. Additionally, our model produces more natural and continuous segmentation masks and is able to capture finer details because it benefits from a dilated spatial pyramid pooling layer that recovers the content lost during encoding by leveraging different dilation rates and aggregating the multiscale feature maps into the decoder. Furthermore, introducing the input image at multiple scales throughout our architecture and introducing supervision at each of these scales helps our model to effectively aggregate the outputs of different stages.

Our technique for estimating the width profiles of retinal vessels by leveraging the generated segmentation masks has also proven to be effective. Its accuracy promises to help in quantifying new relevant biomarkers that correlate with the narrowing and structural changes of vessels.

5 Conclusion

We have presented a novel, fully automated method for retinal vessel segmentation and width estimation. Our deep CNN employs spatial dilated pyramid pooling and introduces the input image at multiple scales with supervision to segment retinal vessels in order to capture the smallest structural details. Our method was tested on two publicly available datasets. It has achieved better than state-of-the-art results in sensitivity and accuracy while being comparable in F1 score on the DRIVE dataset. It also achieves competitive results on the CHASE-DB1 dataset. In addition, we have introduced a method that employs the vessel segmentation maps to estimate the width profiles of retinal vessels. Such information may be very helpful to clinicians as they explore novel biomarkers and in the quantitative assessment of retinal vasculature changes associated with diseases such as diabetes and hypertension.

References

- [1] Abadi, M., Barham, P., Chen, J., Chen, Z., Davis, A., Dean, J., Devin, M., Ghemawat, S., Irving, G., Isard, M., et al.: Tensorflow: A system for large-scale machine learning. In: OSDI. vol. 16, pp. 265–283 (2016) [5](#)
- [2] Akula, A.R., Zhu, S.C.: Visual discourse parsing. arXiv preprint arXiv:1903.02252 (2019) [2](#)
- [3] Alom, M.Z., Hasan, M., Yakopcic, C., Taha, T.M., Asari, V.K.: Recurrent residual convolutional neural network based on U-Net (R2U-Net) for medical image segmentation. arXiv preprint arXiv:1802.06955 (2018) [6](#)
- [4] Fu, H., Xu, Y., Lin, S., Wong, D.W.K., Liu, J.: Deepvessel: Retinal vessel segmentation via deep learning and conditional random field. In: International Conference on Medical Image Computing and Computer-Assisted Intervention. pp. 132–139. Springer (2016) [2](#), [6](#)
- [5] Imran, A., Hatamizadeh, A., Ananth, S.P., Ding, X., Terzopoulos, D., Tajbakhsh, N.: Automatic segmentation of pulmonary lobes using a progressive dense V-network. In: Deep Learning in Medical Image Analysis and Multimodal Learning for Clinical Decision Support, pp. 282–290. Springer (2018), Proc. Fourth MICCAI

International Workshop on Deep Learning in Medical Image Analysis (DLMIA 18) [2](#)

- [6] Jin, Q., Meng, Z., Pham, T.D., Chen, Q., Wei, L., Su, R.: Dunet: A deformable network for retinal vessel segmentation. *Knowledge-Based Systems* (2019) [6](#), [7](#)
- [7] Kachuee, M., Darabi, S., Moatamed, B., Sarrafzadeh, M.: Dynamic feature acquisition using denoising autoencoders. *IEEE Transactions on Neural Networks and Learning Systems* pp. 1–11 (2018) [2](#)
- [8] Laibacher, T., Weyde, T., Jalali, S.: M2U-Net: Effective and efficient retinal vessel segmentation for resource-constrained environments. *arXiv preprint arXiv:1811.07738* (2018) [6](#)
- [9] Li, Q., Feng, B., Xie, L., Liang, P., Zhang, H., Wang, T.: A cross-modality learning approach for vessel segmentation in retinal images. *IEEE Transactions on Medical Imaging* 35(1), 109–118 (2016) [6](#)
- [10] Liskowski, P., Krawiec, K.: Segmenting retinal blood vessels with deep neural networks. *IEEE Transactions on Medical Imaging* 35(11), 2369–2380 (2016) [6](#)
- [11] Melinščak, M., Prentašić, P., Lončarić, S.: Retinal vessel segmentation using deep neural networks. In: *VISAPP 2015 (10th International Conference on Computer Vision Theory and Applications)* (2015) [2](#), [6](#)
- [12] Oliveira, A.F.M., Pereira, S.R.M., Silva, C.A.B.: Retinal vessel segmentation based on fully convolutional neural networks. *Expert Systems with Applications* (2018) [6](#), [7](#)
- [13] Ronneberger, O., Fischer, P., Brox, T.: U-net: Convolutional networks for biomedical image segmentation. In: *Proc. of MICCAI*. pp. 234–241. Springer (2015) [2](#)
- [14] Xie, J., Zheng, Z., Gao, R., Wang, W., Zhu, S.C., Nian Wu, Y.: Learning descriptor networks for 3D shape synthesis and analysis. In: *IEEE Conference on Computer Vision and Pattern Recognition (CVPR)* (June 2018) [2](#)
- [15] Zhang, T.Y., Suen, C.Y.: A fast parallel algorithm for thinning digital patterns. *Communications of the ACM* 27(3), 236–239 (Mar 1984) [5](#)
- [16] Zhuang, J.: LadderNet: Multi-path networks based on U-Net for medical image segmentation. *arXiv preprint arXiv:1810.07810* (2018) [2](#), [6](#)